
A Differential-Geometric Approach to Quantum Ignorance Consistent with Entropic Properties of Statistical Mechanics

Shannon Ray,¹ Paul M. Alsing,¹ Carlo Cafaro,² and H S. Jacinto¹

¹*Information Directorate, Air Force Research Laboratory, Rome, NY 13441, USA*

²*Department of Mathematics and Physics, SUNY Polytechnic Institute, 12203 Albany, New York, USA*

In this paper, we construct the metric tensor and volume for the manifold of purifications associated with an arbitrary reduced density operator ρ_S . We also define a quantum coarse-graining (CG) to study the volume where macrostates are the manifolds of purifications, which we call surfaces of ignorance (SOI), and microstates are the purifications of ρ_S . In this context, the volume functions as a multiplicity of the macrostates that quantifies the amount of information missing from ρ_S . Using examples where the SOI are generated using representations of $SU(2)$, $SO(3)$, and $SO(N)$, we show two features of the CG. (1) A system beginning in an atypical macrostate of smaller volume evolves to macrostates of greater volume until it reaches the equilibrium macrostate in a process in which the system and environment become strictly more entangled, and (2) the equilibrium macrostate takes up the vast majority of the coarse-grained space especially as the dimension of the total system becomes large. Here, the equilibrium macrostate corresponds to maximum entanglement between system and environment. To demonstrate feature (1) for the examples considered, we show that the volume behaves like the von Neumann entropy in that it is zero for pure states, maximal for maximally mixed states, and is a concave function w.r.t the purity of ρ_S . These two features are essential to typicality arguments regarding thermalization and Boltzmann's original CG.

I. INTRODUCTION

In this paper, we introduce a new volume associated with an arbitrary density operator ρ_S that quantifies the ignorance or information missing from ρ_S relative to purifications that can generate it. To compute this volume, we generate all purifications of ρ_S using the method in section 9.2.3 (Uhlmann Fidelity) of [1] and construct the metric tensor of the manifold of purifications. The determinant of the metric tensor gives a volume element which is integrated to compute volume. We then study these volumes by presenting examples for systems whose purifications are generated using unitaries that represent Lie groups $SU(2)$, $SO(3)$, and $SO(N)$. Because these volumes are related to the amount of information missing in ρ_S , we denote the manifolds of purifications as surfaces of ignorance (SOI).

To study the physical properties of our volume, we formulate the SOI as macrostates of an entanglement based quantum coarse-graining (CG) where microstates are the purifications that belong to each SOI; density operators ρ_S are also the macrostates since there is a 1-to-1 correspondence between them and the SOI. The reason for choosing this context is the entanglement entropy has been shown to be closely related to thermal entropy in certain regimes [2–5], and ρ_S can be treated as a reduced density operator, $\rho_S = \text{Tr}_E[|\psi_{ES}\rangle\langle\psi_{ES}|]$, of a closed composite system $|\psi_{ES}\rangle$. Since ρ_S is a reduced density operator of a pure composite system, the von Neumann entropy, S_{VN} , of ρ_S is the entanglement entropy between system, S , and environment, E . This implies that an increase in volume during an entangling process relates to a loss of information from S to E that is reminiscent of an information based thermalization. Although the entanglement entropy is related to thermal entropy, as stated in [6], “it still primarily measures the information

exchange rather than heat exchange.” For this reason, our analysis is not a study of thermalization. Instead, it is an exploration of the SOI and their volumes in the context of “thermalization” as it relates to information exchange/entanglement. Our choice to use CG to study our volume is also justified since using reduced density operators as coarse representations of composite systems is common within the literature [7–12].

With this context in mind, there are two features of Boltzmann's original CG [13] (see Fig. 1) that we demonstrate in the examples of our entanglement coarse-graining (ECG). These features are the following: (1) a system beginning in an atypical macrostate of smaller volume evolves to macrostates of greater volume until it reaches the equilibrium macrostate in a process in which the system and environment become strictly more entangled, and (2) the equilibrium macrostate takes up the vast majority of the coarse-grained space especially as the dimension of the total system becomes large. These features are the basis of typicality arguments for understanding the thermalization of both classical and quantum closed systems [15, 16].

Quantum mechanically, $S_{VN}(|\psi_{ES}\rangle\langle\psi_{ES}|) = 0$ for all evolutions of $|\psi_{ES}\rangle$ in the space of purifications. Therefore, it is common practice [17–19] to demarcate the space of purifications into disjoint sets, or macrostates, for which thermal entropies are defined. For the ECG, the SOI provide this demarcation and their volumes are treated as the multiplicity of a strictly information based “thermal” entropy. It is not our goal to define a quantum Boltzmann entropy, and we are not interested in studying energy or dynamics. Instead, we only analyze volumes and use a purely kinematical approach afforded to us by the ECG. This makes our approach similar to Boltzmann's original analysis and that in [20] which studied the foundations of statistical mechanics in terms of

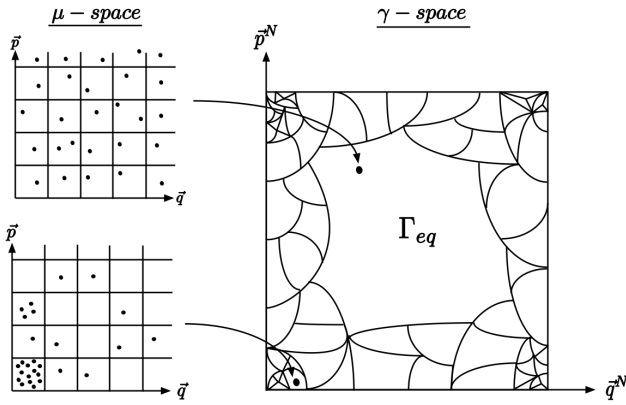


FIG. 1. Illustration of Boltzmann’s original approach to coarse-graining inspired by figure 2 in [14]. On the left are examples of distributions on the single particle phase space, μ -space, while the right depicts the coarse-graining of the $6N$ -dimensional phase space, γ -space. By dividing μ -space into equal cells, macrostates are defined by simply counting the number of particles in each cell. Since each particle is indistinguishable, interchanging which particle occupies each cell does not change the macrostate; thus, there are many equivalent microstates for each macrostate. The size of each macrostate depends on the number of microstates it has. Boltzmann showed that distributions on μ -space that are more uniform have more microstates, and the largest macrostate, Γ_{eq} , is associated with a gas in equilibrium.

entanglement.

To demonstrate feature (1) for the examples considered, we must show that the volume behaves like $S_{VN}(\rho_S)$ in that it is zero for pure state, maximal for maximally mixed states, and is a concave function w.r.t. the purity of ρ_S . This implies that each SOI has a unique entanglement entropy associated with it. It is also consistent with thermalization as described by Boltzmann’s CG where the total system monotonically evolves between macrostates of less volume to macrostates of greater volume until it reaches the most typical macrostate that occupies the vast majority of the coarse-grained space.

In studies that use typicality arguments to understand thermalization, the equilibrium macrostate is defined as the largest macrostate that occupies the vast majority of the coarse-grained space [17–19]. This also defines the equilibrium macrostate for the ECG, but it has the additional trait that its microstates have maximal entanglement between S and E ; this is synonymous with ρ_S being maximally mixed. Therefore, to demonstrate feature (2) we study the average von Neumann entropy of each macrostate belonging to the ECG generated by $SO(3)$ and show that the majority of the coarse-grained space is occupied by the macrostates with maximum or near maximum entanglement entropy. We further show, using $SO(N)$, that the average normalized von Neumann entropy of at least 99.99% of the coarse-grained space tends toward one (maximally mixed) as N becomes large. The

use of 99.99% as a representative value for the vast majority of the coarse-grained space is commonly used in the literature [14, 19, 21, 22].

The final context in which we relate our volume to the multiplicity of a Boltzmann-like entropy is discussed in section IIC of [23] and provided by [24]. In this analysis, Brillouin used the Maxwell demon gedanken to connect negentropy [25, 26] (information) to the Boltzmann entropy. More specifically, he showed that the greater the multiplicity of microstates that are consistent with macrodata, the less information one has about the total system. In our case, the negentropy is defined as

$$I = S_{VN}^{max} - S_{VN}(\rho_S) \quad (1)$$

where S_{VN}^{max} is the von Neumann entropy of the maximally mixed density operator, and ρ_S contains the remaining information of $|\psi_{ES}\rangle$ after the partial trace has been taken. This means if one only has the macrodata contained in ρ_S , they no longer know which purification, i.e. microstate, completes the missing information of ρ_S . Therefore, the greater the volume of the SOI, the more purifications there are which implies one is less likely to successfully guess at random the actual pure state that produced ρ_S . Furthermore, this guess must be random because to use anything other than a maximally mixed distribution on the purifications of ρ_S would, as stated by Jaynes [27], “amount to an arbitrary assumption of information which by hypothesis we do not have.”

The paper is structured as follows. In Sec. II, we construct the metric components and volume of the SOI. In Sec. III, we study the volume in the context of the ECG using unitaries representing Lie groups $SO(3)$, $SU(2)$, and $SO(N)$. In Sec. IV, we generalize the ECG and the metric components of the SOI to include unitary transformations in \mathcal{H}_S . Finally, we conclude in Sec. V with a summary of our results.

II. ENTANGLEMENT COARSE-GRAINING AND THE SURFACES OF IGNORANCE

In this section, we define the macro and microstates of the ECG and derive the metric components and volume of the SOI.

A. Macro and Microstates

In the ECG, macrostates are density operators ρ_S , and microstates are elements of the set of purifications $F^{\rho_S} \equiv \{|\bar{\Gamma}_{ES}^{\rho_S}(\vec{\xi})\rangle\}$ such that

$$\rho_S = \text{Tr}_E \left[|\bar{\Gamma}_{ES}^{\rho_S}(\vec{\xi})\rangle \langle \bar{\Gamma}_{ES}^{\rho_S}(\vec{\xi})| \right]. \quad (2)$$

The space of the environment, \mathcal{H}_E , is taken as a copy of \mathcal{H}_S since it is sufficient to generate all purifications of ρ_S , and $\vec{\xi}$ parameterizes the transformations $U_E(\vec{\xi})$ that represent the Lie group symmetry of \mathcal{H}_E .

Writing ρ_S in its spectral form

$$\rho_S = \sum_{i=1}^N \lambda^i |\lambda_S^i\rangle\langle\lambda_S^i|, \quad (3)$$

where N is the dimension of \mathcal{H}_S , the macrodata are the eigenvalues $\vec{\lambda}$. For an orthonormal basis $\{|\lambda_S^i\rangle\}$ of \mathcal{H}_S , the set of all eigenvalues that satisfy the constraint

$$\sum_{i=1}^N \lambda^i = 1, \quad (4)$$

gives a probability simplex \mathcal{S} where each element of \mathcal{S} is a valid density operator. The probability simplex is a subspace of the projective space $\mathcal{P}(\mathcal{H}_S)$, the latter of which is defined by all normalized rank 1 projectors of \mathcal{H}_S that are well defined up to $U(1)$ symmetries. Since each ρ_S on \mathcal{S} has a unique F^{ρ_S} , there exists a unique ECG of \mathcal{H}_{ES} associated with \mathcal{S} ; this is depicted in Fig. 2 which shows an information/entanglement based ‘‘thermalization’’ process.

To generate F^{ρ_S} we follow the prescription given in 9.2.3 of Wilde’s ‘‘Quantum Information Theory’’ [1]. We begin with the canonical purification

$$|\phi_{ES}^{\rho_S}\rangle = (\hat{1}_E \otimes \sqrt{\rho_S})|\Gamma_{ES}\rangle \quad (5)$$

in \mathcal{H}_{ES} where $\hat{1}_E$ is the identity operator in \mathcal{H}_E ,

$$|\Gamma_{ES}\rangle = \sum_{i=1}^N |\lambda_E^i\rangle|\lambda_S^i\rangle \quad (6)$$

is the unnormalized Bell state, and $\{|\lambda_E^i\rangle\}$ is a copy of $\{|\lambda_S^i\rangle\}$ in \mathcal{H}_E . From here, one can access all purifications by applying unitary transformations associated with the symmetries of \mathcal{H}_E to Eq. 5. This gives,

$$|\bar{\Gamma}_{ES}^{\rho_S}(\vec{\xi})\rangle = (U_E(\vec{\xi}) \otimes \hat{1}_S)|\phi_{ES}^{\rho_S}\rangle = (U_E(\vec{\xi}) \otimes \sqrt{\rho_S})|\Gamma_{ES}\rangle. \quad (7)$$

In general, \mathcal{H}_E need not be a copy of \mathcal{H}_S since ρ_S can be derived from any bipartition of an arbitrary many-body system $|\psi_{ES}\rangle$. Therefore, to generalize the macrostates of the ECG given by Eq. 7 to an arbitrary purification space $\mathcal{H}_{\bar{E}S}$ where $\mathcal{H}_{\bar{E}} \neq \mathcal{H}_S$, we use the fact that all purifications of ρ_S are unitarily related.

Given the restriction that $\dim(\bar{E}) \geq N$, the ECG of \mathcal{H}_{ES} can be extended to $\mathcal{H}_{\bar{E}S}$ by

$$|\bar{\Gamma}_{\bar{E}S}^{\rho_S}(\vec{\xi})\rangle = (U_{E \rightarrow \bar{E}} \otimes \hat{1}_S)|\bar{\Gamma}_{ES}^{\rho_S}(\vec{\xi})\rangle \quad (8)$$

where

$$U_{E \rightarrow \bar{E}} = \sum_{i=1}^N |\lambda_{\bar{E}}^i\rangle\langle\lambda_E^i| \quad (9)$$

and $\{|\lambda_{\bar{E}}^i\rangle\}$ is a complete orthonormal basis of $\mathcal{H}_{\bar{E}}$. Since all macrostates of \mathcal{H}_{ES} can be extended to macrostates of some larger $\mathcal{H}_{\bar{E}S}$, we only need to consider the former to define a general ECG.

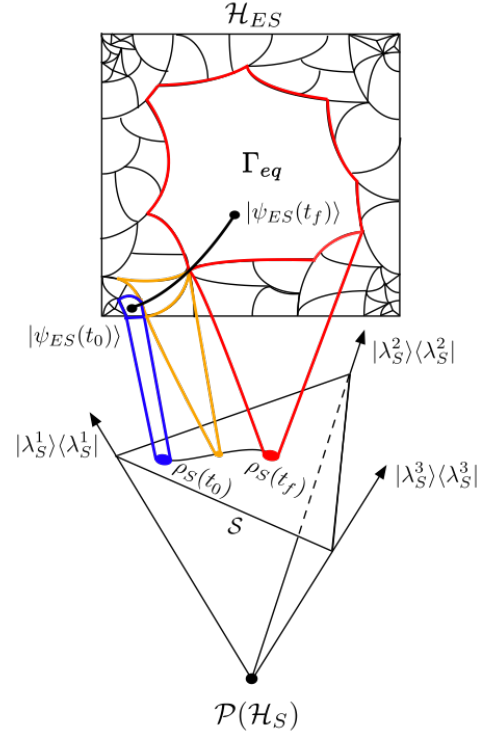


FIG. 2. A conceptual example of an entangling process between ρ_S and ρ_E . From the perspective of ρ_S , $|\psi_{ES}\rangle$ evolves from macrostates F^{ρ_S} with smaller volume to F^{ρ_S} with larger volume. If an observer only has access to the information in ρ_S , they can’t resolve the actual state of $|\psi_{ES}\rangle$ beyond the SOI depicted by the blue, orange, and red macrostates. For a global observer with access to $|\psi_{ES}\rangle$, the entangling process is a continuous curve of pure states from $|\psi_{ES}(t_0)\rangle$ to $|\psi_{ES}(t_f)\rangle$. This is the black curve in \mathcal{H}_{ES} . Each $\rho_S \in \mathcal{S} \subset \mathcal{P}(\mathcal{H}_S)$ has one unique $F^{\rho_S} \subset \mathcal{H}_{ES}$. This implies a unique coarse-graining of \mathcal{S} in \mathcal{H}_{ES} .

B. Surfaces of Ignorance: Metric Components and Volume

To compute the metric components and volume associated with F^{ρ_S} , we construct its first fundamental form using a Taylor expansion of Eq. 7. Expanding around parameters $\vec{\xi}_0$ using $\vec{\xi}$, the displacement vector is given by $d\vec{\xi} = \vec{\xi} - \vec{\xi}_0$. Taking the Taylor expansion of $|\bar{\Gamma}_{ES}^{\rho_S}(\vec{\xi})\rangle$ to first order, and bringing the zeroth order term to the l.h.s, the differential is given by

$$|d\bar{\Gamma}\rangle \equiv |\bar{\Gamma}(\vec{\xi}_0 + d\vec{\xi})\rangle - |\bar{\Gamma}(\vec{\xi}_0)\rangle = \sum_{i=1}^n |\bar{\Gamma}_{,\xi_i}\rangle d\xi_i \quad (10)$$

where n is the number of parameters of the unitary representation of the Lie groups and $|\bar{\Gamma}_{,\xi_i}\rangle$ is the partial derivative of $|\bar{\Gamma}\rangle$ w.r.t ξ_i . For the remainder of the paper, superscript ρ_S and subscript ES will be dropped from $|\bar{\Gamma}_{ES}^{\rho_S}(\vec{\xi})\rangle$ for simplicity of notation. Since we are working in \mathcal{H}_{ES} , and all of our states are pure, the scalar product is well defined. The components g_{ij} of the metric tensor

\mathbf{g} induced by the scalar product are given by the first fundamental form

$$ds^2 = \langle d\bar{\Gamma} | d\bar{\Gamma} \rangle = \sum_{i,j=1}^n \langle \bar{\Gamma}_{,i} | \bar{\Gamma}_{,j} \rangle d\xi_i d\xi_j \quad (11)$$

where $g_{ij} = \langle \bar{\Gamma}_{,i} | \bar{\Gamma}_{,j} \rangle$. From Eq. 11, the volume element is $dV = \sqrt{\text{Det}[\mathbf{g}]} d\xi_1 d\xi_2 \dots d\xi_n$ and the volume is

$$V = \int_{\xi_1} \int_{\xi_2} \dots \int_{\xi_n} dV. \quad (12)$$

III. VOLUME EXAMPLES

In this section, we give explicit expressions of volume for the examples considered and compare them to the von Neumann entropy, $S_{VN} = -\sum_{i=1}^N \lambda^i \log \lambda^i$, and the linear entropy, $S_L = 1 - \text{Tr}[\rho_S^2]$. We demonstrate feature (1) of Boltzmann's original CG for $SU(2)$, features (1) and (2) for $SO(3)$, and extend the demonstration of feature (2) for $SO(3)$ in the limit of large N using $SO(N)$. But first, we give the expressions for arbitrary unitary transformations that will be used to compute the metric components and volumes for our examples.

A. Arbitrary N -Dimensional Unitary Transformations

Following the prescription in [28], any arbitrary N -dimensional unitary transformation can be written as successive transformations of 2-dimensional subspaces. Let $E^{(i,j)}(\phi_{ij}, \psi_{ij}, \chi_{ij})$ be an arbitrary transformation about the (i, j) -plane. Its components are

$$\begin{aligned} E_{kk}^{(i,j)} &= 1 & k = 1, \dots, d & \quad k \neq i, j \\ E_{ii}^{(i,j)} &= e^{i\psi_{ij}} \cos \phi_{ij} \\ E_{ij}^{(i,j)} &= e^{i\chi_{ij}} \sin \phi_{ij} \\ E_{ji}^{(i,j)} &= -e^{-i\chi_{ij}} \sin \phi_{ij} \\ E_{jj}^{(i,j)} &= e^{-i\psi_{ij}} \cos \phi_{ij} \end{aligned} \quad (13)$$

and zero everywhere else. The superscript indices (i, j) index the 2-D plane about which the transformation is applied, and the subscripts are the nonzero matrix indices. From here, one can construct successive transformations

$$\begin{aligned} E_1 &= E^{(1,2)}(\phi_{12}, \psi_{12}, \chi_{12}) \\ E_2 &= E^{(2,3)}(\phi_{23}, \psi_{23}, 0) E^{(1,3)}(\phi_{13}, \psi_{13}, \chi_{13}) \\ &\vdots \\ &\vdots \\ E_{N-1} &= E^{(N-1,N)}(\phi_{N-1,N}, \psi_{N-1,N}, 0) \\ &\quad E^{(N-2,N)}(\phi_{N-2,N}, \psi_{N-2,N}, 0) \\ &\quad \dots E^{(1,N)}(\phi_{1N}, \psi_{1N}, \chi_{1N}) \end{aligned} \quad (14)$$

$$\dots E^{(1,N)}(\phi_{1N}, \psi_{1N}, \chi_{1N}) \quad (15)$$

and finally an arbitrary $U(N)$ transformation

$$U = e^{i\alpha} E_1 E_2 \dots E_{N-1} \quad (16)$$

where $\phi_{ij} \in [0, \pi/2]$ and $\alpha, \psi_{ij}, \chi_{ij} \in [0, 2\pi]$. With the arbitrary unitaries defined, we now present our examples.

B. Example: $SU(2)$

Here we demonstrate feature (1) for $SU(2)$ by computing the volume and comparing it to the von Neumann and linear entropies. We do not attempt to demonstrate feature (2) since it is a feature that manifests for large systems and here the composite system is only four dimensional.

From Eq. 16 the unitaries of $SU(2)$ are given by

$$U(\phi, \psi, \chi) = \begin{bmatrix} e^{i\psi} \cos \phi & e^{i\chi} \sin \phi \\ -e^{-i\chi} \sin \phi & e^{-i\psi} \cos \phi \end{bmatrix} \quad (17)$$

where $N = 2$, $\alpha = 0$, $\psi, \chi \in [0, 2\pi]$, $\phi \in [0, \pi/2]$, and the subscript 12 in the angles is dropped since the example is only 2-dimensional. Computing the metric components directly, the nonzero values of the metric are

$$g_{\phi\phi} = \lambda^1 + \lambda^2 \quad (18)$$

$$g_{\psi\psi} = (\lambda^1 + \lambda^2) \cos^2 \phi \quad (19)$$

$$g_{\chi\chi} = (\lambda^1 + \lambda^2) \sin^2 \phi \quad (20)$$

$$g_{\phi\psi} = g_{\phi\chi} = i(\lambda^1 - \lambda^2) \cos \phi \sin \phi. \quad (21)$$

Taking the $\sqrt{\text{Det}(\mathbf{g})}$ and substituting $\lambda^2 = 1 - \lambda^1$ gives

$$dV_{SU(2)} = \sqrt{\lambda^1(1 - \lambda^1)} \sin 2\phi d\phi d\psi d\chi \quad (22)$$

and integrating over $\{\phi, \psi, \chi\}$ gives

$$V_{SU(2)} = 4\pi^2 \sqrt{\lambda^1(1 - \lambda^1)} = 4\pi^2 \sqrt{S_L/2} \quad (23)$$

where $\lambda^2 = 1 - \lambda^1 = \frac{1}{2} \left[1 + \sqrt{2 \text{Tr}[\rho^2] - 1} \right]$.

We compare the normalized volume, $V_{SU(2)}^{\text{norm}}$, with the normalized von Neumann entropy, S_{VN}^{norm} , and normalized linear entropy, S_L^{norm} , in Fig. 3. Each volume/entropy is normalized w.r.t their maximum values so that they take values on the interval $[0, 1]$. It is shown that all three functions are zero on pure states, maximal on maximally mixed states, and are concave function w.r.t. the purity of ρ_S . This shows that feature (1) is satisfied for this example. In fact, the volume is an upper bound of both entropies. It should also be noted that the behavior of $V_{SU(2)}^{\text{norm}}$ deviates from S_{VN}^{norm} and S_L^{norm} in that it is flatter near maximally mixed states and steeper near pure states. As we will see in Sec. III C, this flatter behavior has implications about feature (2) also being satisfied in that more of the coarse-grained space consists of macrostates with greater von Neumann entropy. But, one would not expect this feature to be pronounced since the dimension of this example is so low.

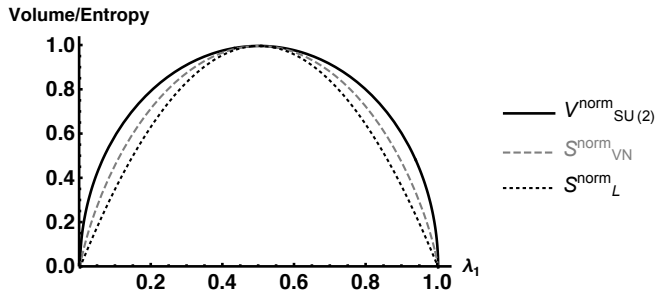


FIG. 3. Plot of the normalized volume, von Neumann, and linear entropies for 2-level systems whose purifications are generated using $SU(2)$.

C. Example: $SO(3)$

This section is broken into two subsections. In Sec. III C 1, we demonstrate feature (1) by computing volume and comparing it to the linear and von Neumann entropies. In Sec. III C 2, we demonstrate feature (2) by discretizing \mathcal{S} to construct an explicit CG. We then compute the average von Neumann entropy of each discrete macrostate and show that a significant majority of the coarse-grained space consists of macrostates with maximum or near maximum von Neumann entropy which is consistent with the composite system being maximally entangled.

1. Computing Volume

From Eq. 16, the unitaries associated with $SO(3)$ are given by choosing $N = 3$ and $\alpha = \psi_{ij} = \chi_{ij} = 0$ for all i and j . This leaves parameters $\vec{\xi} = (\phi_{12}, \phi_{13}, \phi_{23})$ where $\phi_{12}, \phi_{13}, \phi_{23} \in [0, \pi/2]$. The resulting unitaries are given by

$$U(\phi_{12}, \phi_{13}, \phi_{23}) = \begin{bmatrix} \cos \phi_{12} \cos \phi_{13} - \sin \phi_{12} \sin \phi_{13} \sin \phi_{23} & \cos \phi_{23} \sin \phi_{12} & \cos \phi_{12} \sin \phi_{13} + \cos \phi_{13} \sin \phi_{12} \sin \phi_{23} \\ -\cos \phi_{13} \sin \phi_{12} - \cos \phi_{12} \sin \phi_{13} \sin \phi_{23} & \cos \phi_{12} \cos \phi_{23} & -\sin \phi_{12} \sin \phi_{13} + \cos \phi_{12} \cos \phi_{13} \sin \phi_{23} \\ -\cos \phi_{23} \sin \phi_{13} & -\sin \phi_{23} & \cos \phi_{13} \cos \phi_{23} \end{bmatrix}. \quad (24)$$

Since $U(\phi_{12}, \phi_{13}, \phi_{23})$ are the unitaries of both \mathcal{H}_E and \mathcal{H}_S , we will use the sub-labels E and S to keep track of which space U is acting upon.

Working in the basis of \mathcal{S} , $\{|\lambda_S^i\rangle\}$ is given by

$$\{|\lambda_S^i\rangle\} = \left\{ \begin{bmatrix} 1 \\ 0 \\ 0 \end{bmatrix}, \begin{bmatrix} 0 \\ 1 \\ 0 \end{bmatrix}, \begin{bmatrix} 0 \\ 0 \\ 1 \end{bmatrix} \right\}. \quad (25)$$

This gives an explicit form of the unnormalized Bell state

given by Eq. 6. From here, all purifications are generated by

$$|\bar{\Gamma}(\vec{\xi})\rangle = \sum_{i=1}^3 \sqrt{\lambda^i} U_E(\vec{\xi}) |\lambda_E^i\rangle \otimes |\lambda_S^i\rangle. \quad (26)$$

Using Eq. 26, the nonzero metric components of $F^{ps} \equiv \{|\bar{\Gamma}(\vec{\xi})\rangle\}$ are

$$g_{\phi_{12}\phi_{12}} = \langle \bar{\Gamma}_{,\phi_{12}} | \bar{\Gamma}_{,\phi_{12}} \rangle = \sin^2 \phi_{23} + \frac{1}{4} (\lambda^1 + \lambda^2 + 3(\lambda^1 + \lambda^2) \cos 2\phi_{23} + 2(\lambda^1 - \lambda^2) \cos 2\phi_{13} \sin^2 \phi_{23}) \quad (27)$$

$$g_{\phi_{13}\phi_{13}} = \langle \bar{\Gamma}_{,\phi_{13}} | \bar{\Gamma}_{,\phi_{13}} \rangle = \lambda^1 + \lambda^2 \quad (28)$$

$$g_{\phi_{23}\phi_{23}} = \langle \bar{\Gamma}_{,\phi_{23}} | \bar{\Gamma}_{,\phi_{23}} \rangle = \frac{1}{2} (2 - \lambda^1 - \lambda^2 - (\lambda^1 - \lambda^2) \cos 2\phi_{13}) \quad (29)$$

$$g_{\phi_{12}\phi_{13}} = g_{\phi_{13}\phi_{12}} = \langle \bar{\Gamma}_{,\phi_{12}} | \bar{\Gamma}_{,\phi_{13}} \rangle = (\lambda^1 + \lambda^2) \cos \phi_{23} \quad (30)$$

$$g_{\phi_{12}\phi_{23}} = g_{\phi_{23}\phi_{12}} = \langle \bar{\Gamma}_{,\phi_{12}} | \bar{\Gamma}_{,\phi_{23}} \rangle = -(\lambda^1 - \lambda^2) \cos \phi_{13} \sin \phi_{23} \sin \phi_{13} \quad (31)$$

where $g_{\phi_{13}\phi_{23}} = g_{\phi_{23}\phi_{13}} = 0$. Taking $\sqrt{\text{Det}(\mathbf{g})}$ gives

$$\frac{dV_{SO(3)}}{d\phi_{12}d\phi_{13}d\phi_{23}} = \sqrt{(\lambda^1 + \lambda^2)(\lambda^1 + \lambda^3)(\lambda^2 + \lambda^3)} \cos \phi_{23} \quad (32)$$

and integrating over $\vec{\xi}$ gives

$$V_{SO(3)} = (\pi^2/4) \sqrt{(\lambda^1 + \lambda^2)(\lambda^1 + \lambda^3)(\lambda^2 + \lambda^3)} \quad (33)$$

$$= (\pi^2/4) \sqrt{(1 - \lambda^1)(1 - \lambda^2)(\lambda^1 + \lambda^2)} \quad (34)$$

where the second equality is due to the constraint that the sum of the eigenvalues must equal one.

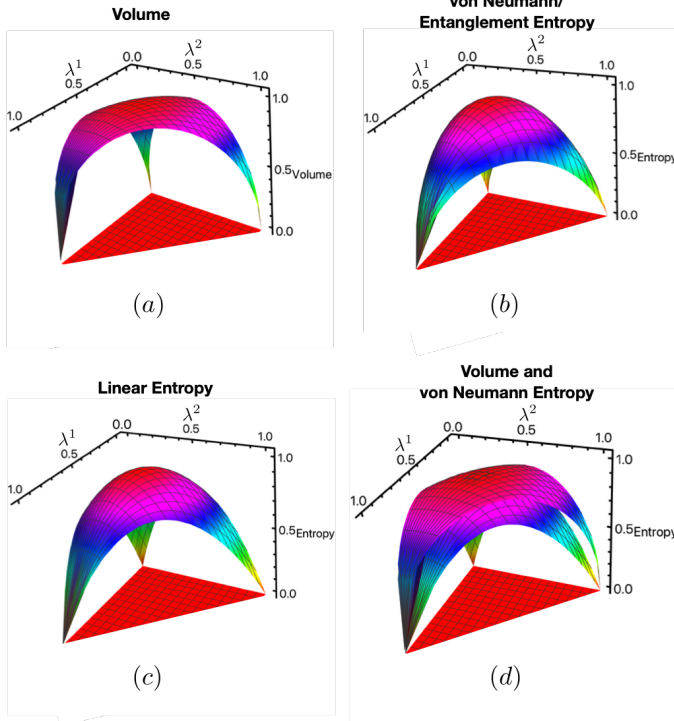


FIG. 4. Comparison between the normalizations of $V_{SO(3)}$, von Neumann entropy, and linear entropy. This demonstrates that $V_{SO(3)}$ satisfies feature (1) of Boltzmann’s original CG for the example considered.

Like the $SU(2)$ example, we compare the normalized volume, $V_{SO(3)}^{\text{norm}}$, with S_{VN}^{norm} and S_L^{norm} by plotting them in Fig. 4. Here we see, as was seen for $SU(2)$, that $V_{SO(3)}^{\text{norm}}$ is zero for pure states, maximal on maximally mixed states, and concave w.r.t purity thus satisfying feature (1). Also like the $SU(2)$ example, the volume upper bounds S_{VN}^{norm} as seen in Fig. 4d. It also upper bounds S_L^{norm} , but we do not show it for sake of clarity. Notice as well that $V_{SO(3)}^{\text{norm}}$ is flatter near the maximally mixed state and steeper near pure states. This again is an indication that it also satisfies feature (2) which we analyze explicitly in Sec. IIIC 2.

2. Analyzing Entanglement Entropy of Macrostates

To demonstrate feature (2) for $SO(3)$, we compute the fraction of \mathcal{S} that belongs to each macrostate in the coarse-grained space, \mathcal{H}_{ES} , and compute the average von Neumann entropy of each fraction. The purpose is to show that the greatest fraction belongs to macrostates with maximum or near maximum von Neumann entropy which, again, is consistent with maximal entanglement between system and environment. However, since ρ_S , F^{ρ_S} , and $V_{SO(3)}^{\text{norm}}$ are continuous functions of eigenvalues

$\vec{\lambda}$, distinct macrostates are not well defined. To resolve this problem, we discretize \mathcal{S} into discrete density operators, ρ_l , of equal area, and we discretize the range of $V_{SO(3)}^{\text{norm}}$, $L = [0, 1]$, into discrete segments of equal length L_a . With these discretizations, L_a represent the discrete macrostates in \mathcal{H}_{ES} to which fractions of \mathcal{S} belong.

The proposed discretizations have two benefits. First, it allows us to identify ρ_l with segments L_a based on their volumes in \mathcal{H}_{ES} and compute

$$\mathcal{S}_a = \frac{|L_a|}{|\rho_l|} \quad (35)$$

where $|L_a|$ is the number of ρ_l belonging to L_a and $|\rho_l|$ is the total number of discrete density operators; this gives the fraction of \mathcal{S} that belongs to each macrostate in \mathcal{H}_{ES} . Second, it allows us to compute the average normalized von Neumann entropy of each \mathcal{S}_a

$$\overline{S_{VN}^{\text{norm}}}(\mathcal{S}_a) = \frac{\sum_{i=1}^{|L_a|} S_{VN}^{\text{norm}}(\rho_i)}{|L_a|} \quad (36)$$

where ρ_i belong to L_a . We then look at each \mathcal{S}_a and its $\overline{S_{VN}^{\text{norm}}}(\mathcal{S}_a)$ to see if feature (2) is demonstrated. Additionally, since $S_{VN}^{\text{norm}}(\vec{\lambda})$, $S_L^{\text{norm}}(\vec{\lambda}) \in L$, we can compute Eqs. 35 and 36 for them as well except we replace volume with entropies when sorting ρ_l into macrostates L_a . This allows us to compare them directly to $V_{SO(3)}^{\text{norm}}$ which provides additional evidence that feature (2) is uniquely demonstrated by the ECG.

The probability simplex \mathcal{S} is discretized into finite ρ_l of equal area by uniformly sampling it using the transformation

$$\lambda^1 = 1 - \sqrt{\eta^1} \quad (37)$$

$$\lambda^2 = \sqrt{\eta^1}(1 - \eta^2) \quad (38)$$

$$\lambda^3 = \sqrt{\eta^1}\eta^2, \quad (39)$$

where $\eta^1, \eta^2 \in [0, 1]$ are uniformly distributed in the unit interval, as seen in [29]. Dividing η^1 and η^2 into ℓ equal segments and transforming back to the $\vec{\lambda}$ basis divides \mathcal{S} into ℓ^2 discrete ρ_l , where $l \in [1, \ell^2]$; this is shown in Fig. 5b. The interval $L = [0, 1]$ is discretized by dividing it into k equal segments, L_a , where a is an integer between $[1, k]$; this is shown in Fig. 5c. Given the discretization of \mathcal{S} and L , one can compute Eqs. 35 and 36.

Choosing $\ell = 300$ and $k = 10$, we compute $V_{SO(3)}^{\text{norm}}$, S_L^{norm} , and S_{VN}^{norm} at the center of squares in the $\vec{\eta}$ basis and assign that value to the corresponding ρ_l in the $\vec{\lambda}$ basis. From Fig. 5a, we see that the distance from the center of a given square is given by $dl = 1/(2\ell)$. As ℓ goes to infinity, dl goes to zero, and the volume/entropies associated with the ρ_l in the $\vec{\lambda}$ basis becomes more representative of the actual value at the center.

Coloring each ρ_l using a colormap derived from the volume and entropies assigned to them gives the first row of Fig. 6. Notice how this simply produces the contour plots of Fig. 4. To show the fraction of \mathcal{S} associated

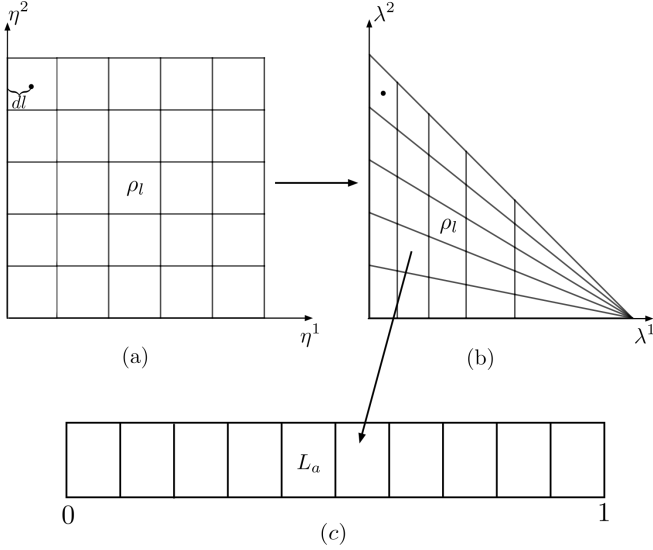


FIG. 5. Discretization of the probability simplex \mathcal{S} into discrete ρ_l of equal area, and interval $L = [0, 1]$ into segments of equal length for $\ell = 5$ and $k = 10$. In (a), we have the division of \mathcal{S} in the $\vec{\eta}$ basis while (b) is in the $\vec{\lambda}$ basis; the transformation is given by Eqs. 37 - 39. In (c), we have the sorting of ρ_l into volume equivalent classes L_a .

with L_a , we assign an arbitrary color to each L_a and color the ρ_l in accordance with the L_a in which they belong; this gives the second row of Fig. 6. There is nothing special about the choice of colors; they are only meant to distinguish L_a . Computing Eq. 35 and plotting the results gives the third row in Fig. 6. Due to the triangular distortions of \mathcal{S} by the transformation from $\vec{\eta}$ to $\vec{\lambda}$, these plots are produced with the restriction that $\eta^1 \in (1/4, 1]$ and $\eta^2 \in (1/2, 1]$. This guarantees the data in the analysis is within Weyl chambers [30] that do not include the triangular distortions [31] of the grid in the $\vec{\lambda}$ basis. Finally, the fourth row of Fig. 6 is given by Eq. 36.

Looking at rows 3 and 4 of the first column of Fig. 6, we see that over sixty percent of \mathcal{S} consists of ρ_l belonging to L_{10} . These are states for which $V_{SO(3)}^{\text{norm}} \geq 0.9$. Furthermore, the average normalized von Neumann entropy of this class is 0.88 bits. This shows that the average entanglement entropy associated with L_{10} is near maximal. These results are in stark contrast to the von Neumann and linear entropies whose L_{10} segments make up less than thirty three percent of the total volume. This is significant because it shows that the von Neumann and linear entropies perform worse than the volume when reproducing feature (2) which is that most of the space of states consist of states near equilibrium. This suggests that the volumes of the ECG uniquely captures features of a CG that is related to thermalization.

For Boltzmann's original CG, over 99.99% of γ -space consists of states at equilibrium. This is because it is assumed that one is working with a high dimensional system with a number of particles on the order of Avogadro's

number. In this example, we are only working with 3-level systems so the dimension of the space is vastly less. Nonetheless, we still showed that the majority of \mathcal{H}_{ES} consists of states near equilibrium. In Sec. III D, we compute $\overline{S_{VN}^{\text{norm}}}$ for states that occupy at least 99.99% of the volume of \mathcal{H}_{ES} and show that it tends toward one (maximum entanglement) as the dimension of the system increases.

D. Example: $SO(N)$

To extend the results from Sec. III C 2, we first provide an expression for $V_{SO(N)}^{\text{norm}}$. We then use marginal density operators

$$\rho_S(\lambda^1) = \lambda^1 |\lambda^1\rangle \langle \lambda^1| + \frac{1 - \lambda^1}{N - 1} \sum_{i=2}^N |\lambda^i\rangle \langle \lambda^i|, \quad (40)$$

which are mixtures of a pure state and the maximally mixed state (of dimension $N - 1$), to simplify the previous analysis for higher dimensions. This allows us to write $V_{SO(N)}^{\text{norm}}$ as a function of λ^1 . We then identify the value λ^{1*} below which at least 99.99% of the volume exists. From here, the average normalized von Neumann entropy for $\rho_S(\lambda^1)$ between $\lambda^1 \in [1/N, \lambda^{1*}]$ is computed. The purpose is to show that the average normalized von Neumann entropy for at least 99.99% of the coarse-grained space parameterized by λ^1 tends to one (maximal entanglement) as the dimension, N , of the system increases.

We compute the volume for $SO(2)$ – $SO(5)$ to construct $V_{SO(N)}$ by induction. The volume associated with $SO(2)$ is computed by setting $\psi = \xi = 0$ in Eq. 17; this gives one metric component $dV_{SO(2)} = \sqrt{\lambda^1 + \lambda^2} d\phi$. Inserting $dV_{SO(2)}$ into Eq. 12 and integrating ϕ from zero to $\pi/2$ gives

$$V_{SO(2)} = (\pi/2) \sqrt{\lambda^1 + \lambda^2} = \pi/2. \quad (41)$$

This result is trivial and uninteresting since $\lambda^1 + \lambda^2 = 1$, but it does provide necessary information for inferring the general form of $V_{SO(N)}$.

Although we have an analytical form of $dV_{SO(4)}$ produced by mathematica, it can't be simplified to a clean form like Eqs. 22 and 32 when the number of parameters, $\vec{\xi}$, is greater than three [32]. To overcome this obstacle, we simplify $dV_{SO(4)}$ by setting $\vec{\xi} = 0$. This is done because we noticed that the volume elements $dV_{SO(3)}$, $dV_{SU(2)}$, and $dV_{SO(2)}$ are products between functions of λ 's and functions of $\vec{\xi}$, which may imply that volumes of the surfaces are product measures as seen in [30]. As such, the $\vec{\lambda}$ portion of the volume is removed from the integral, and the exact volume is merely scaled by factors of π . Assuming $dV_{SO(4)}$ is merely a product between a function of $\vec{\lambda}$ and cosines like Eq. 32, we set $\vec{\xi} = 0$ to

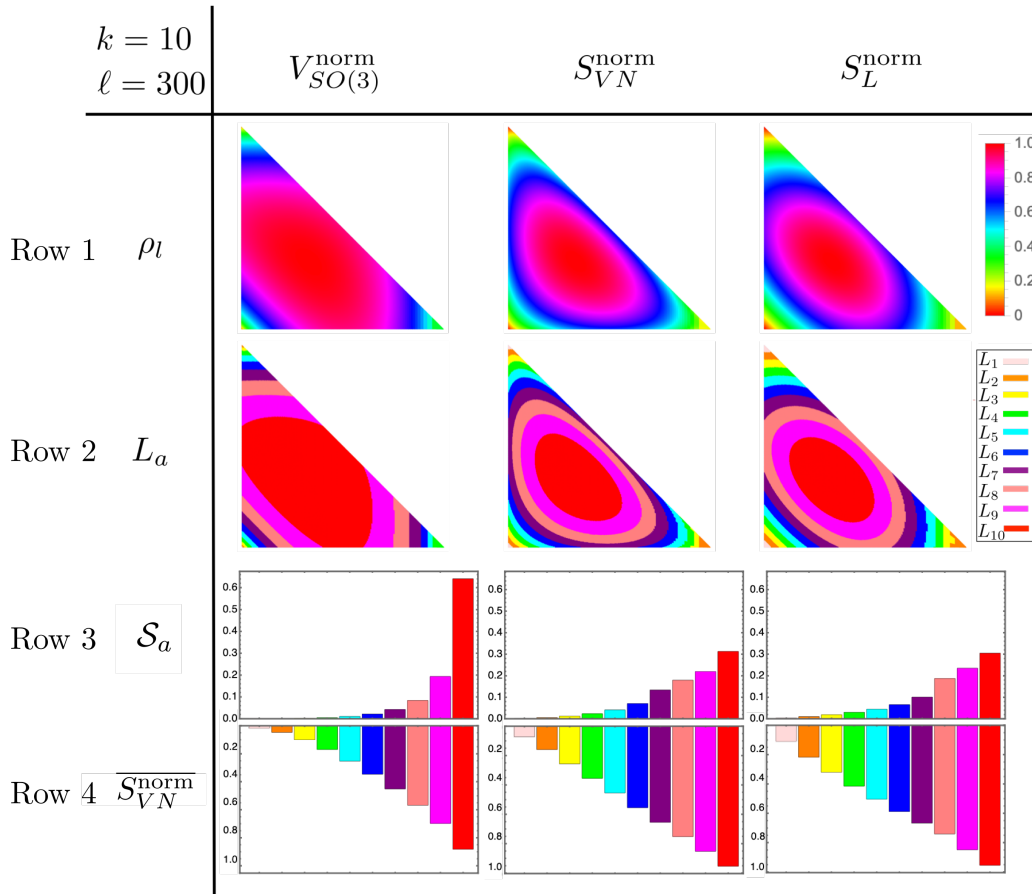


FIG. 6. Results of coarse-graining $\mathcal{H}_{ES} = \mathbb{R}^3 \otimes \mathbb{R}^3$. Row one is the discretization of \mathcal{S} where each ρ_l is colored using the volume or entropy of each column. Row two is the result of discretizing the interval $L = [0, 1]$ and sorting equivalent ρ_l into segments L_a . Row three is the fraction of ρ_l belonging to each L_a . Finally, row four is the average von Neumann entropy of each L_a . It should be noted that the data from the graphs does not include the triangular distortions caused by the discretization of \mathcal{S} . We only used data from Weyl chambers that do not include triangles.

simplify it. Making this simplification gives

$$\frac{dV_{SO(N)}|_{\vec{\xi}=0}}{d\xi_1 d\xi_2 \dots d\xi_{N(N-1)/2}} = \prod_{i < j}^N \sqrt{\lambda^i + \lambda^j} \quad (42)$$

where $N = 4$ and $N(N-1)/2$ is the number of parameters of $SO(N)$. Next, we justify the choice of setting $\vec{\xi} = 0$ as valid by numerically computing $V_{SO(4)}$ directly, without setting $\vec{\xi} = 0$, and compare it to Eq. 42 for $N = 4$.

Comparing the volumes given by Eq. 42 with the direct numerical integration of $V_{SO(4)}$ where $\vec{\xi} \neq 0$ and the full integration over $\vec{\xi}$ is performed gives Fig. 7. This result numerically shows that Eq. 42 (normalized to maximum) is a very good approximation of the actual normalized volume and that they may be in fact the same. This is not a proof, but it is a strong indication that the assumption leading to Eq. 42 is valid. We also computed $dV_{SO(5)}$ and set $\vec{\xi} = 0$ and got the same result for $SO(4)$ which is that the volume, barring factors of π , is merely the square root of the product of all pairwise sums of eigenvalues. Using

these results, along with $V_{SO(2)}$ and $V_{SO(3)}$, we infer by induction that

$$V_{SO(N)} = \prod_{i < j}^N \sqrt{\lambda^i + \lambda^j}. \quad (43)$$

Now that we have a general form of $V_{SO(N)}$, we proceed with our procedure to extend the results from Sec. III C 2.

Inserting the choice of eigenvalues consistent with $\rho_S(\lambda^1)$ into Eq. 43 and normalizing w.r.t the maximum volume gives

$$V_{SO(N)}^{\text{norm}}(\lambda^1) = \frac{\left(\lambda^1 + \frac{1-\lambda^1}{N-1}\right)^{\frac{N-1}{2}} \left(2\frac{1-\lambda^1}{N-1}\right)^{\frac{(N-1)(N-2)}{4}}}{\left(\frac{2}{N}\right)^{\frac{N(N-1)}{4}}}. \quad (44)$$

To show that the majority of \mathcal{H}_{ES} increasingly tends toward maximally entangled states (maximum von Neumann entropy of ρ_S), we plot Eq. 44 for $N = 3, 5, 7, 11$, and 30 in Fig. 8. We see that the centroid of each plot tends toward states with maximum von Neumann

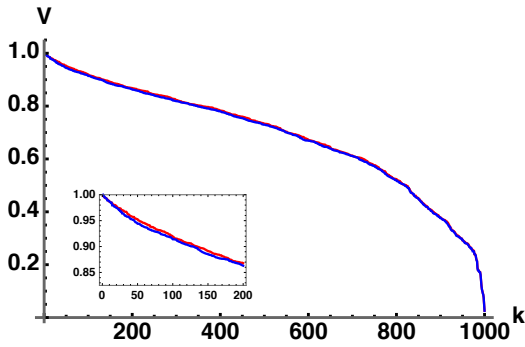


FIG. 7. Plot comparing volumes given by Eq. 42 with direct numerical integration of $dV_{SO(4)}$. Both are normalized on their maximum values. To generate the plots, one thousand $\vec{\lambda}$'s were selected uniformly by generalizing Eqs. 37-39 to four dimensions and computing the corresponding volume. The list of volumes and eigenvalues are sorted, $k \in [1, 1000]$, from largest to smallest. The red plot was computed from Eq. 42, and the blue plot is a direct integration of $dV_{SO(4)}$ using Monte Carlo integration. The inset is given to show that the plots are not exact but very close.

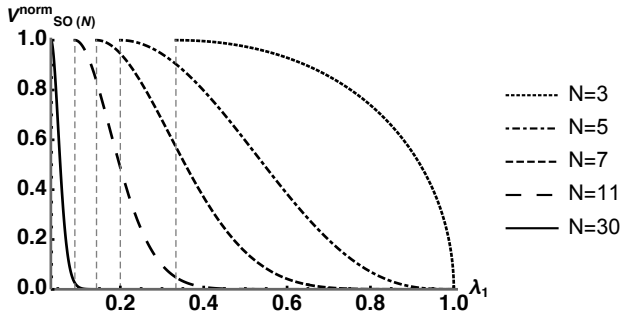


FIG. 8. Plot of $V_{SO(N)}^{\text{norm}}$ for $N = 3, 5, 7, 11, 30$. The dashed vertical lines are located at the minimal value of λ^1 for each plot, which is $1/N$, the maximally mixed state. Notice how the centroids tend toward maximally mixed states as pure states subsume less volume as N increases.

entropy as N increases. To quantify these results, we identify the value λ^{1*} for various values of N where $V_{SO(N)}^{\text{norm}}(\lambda^{1*}) = 10^{-4}$. For the values of N used, this choice of λ^{1*} guarantees that

$$\frac{\int_{1/N}^{\lambda^{1*}} V_{SO(N)}^{\text{norm}}(\lambda^1) d\lambda^1}{\int_{1/N}^1 V_{SO(N)}^{\text{norm}}(\lambda^1) d\lambda^1} > 0.9999, \quad (45)$$

where $\lambda^1 = 1/N$ indicates the maximally mixed $\rho_S(\lambda^1)$. Plotting the average normalized von Neumann entropy with $\lambda^1 \in [1/N, \lambda^{1*}]$ as a function of N gives Fig. 9. This clearly shows that the average normalized von Neumann entropy for at least 99.99% of \mathcal{H}_{ES} parameterized by λ^1 tends toward 1 as N becomes large. This implies that the vast majority of the coarse-grained space consists of equilibrium macrostates which are characterized by maximum entanglement entropy.

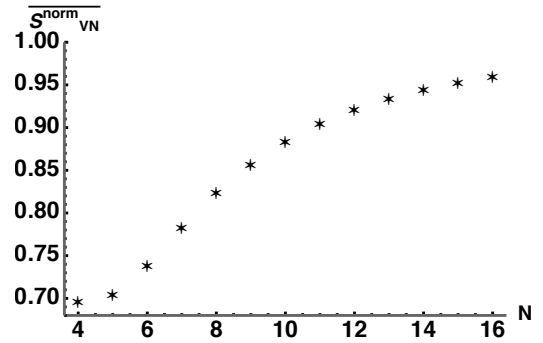


FIG. 9. Plot of the average von Neumann entropy (normalized to the maximally mixed state) with $\lambda^1 \in [1/N, \lambda^{1*}]$ as a function of N . This quantifies the results of Fig. 8 by showing that the average von Neumann entropy of states whose volumes take over 99.99% of \mathcal{H}_{ES} tends toward 1 where 1 corresponds to maximum entanglement entropy.

From this analysis, we have demonstrated feature (1) of Boltzmann's CG for $SU(2)$ and $SO(3)$ by comparing them to the von Neumann and linear entropies in Figs. 3 and 4, respectively. We also demonstrated feature (2) for $SO(3)$ by constructing an explicit CG and computing the average entanglement entropy of each macrostate and extended it to $SO(N)$ using marginal density operators given by Eq. 8. We did not include an analysis of $SU(N)$ since computing the determinant of the metric becomes prohibitively difficult as the number of parameters, $\vec{\xi}$, increases [32].

IV. GENERALIZING THE ENTANGLEMENT COARSE-GRAINING

In this section we generalize our formalism to include unitary transformation of \mathcal{S} in $\mathcal{P}(\mathcal{H}_S)$. This allows us to define the metric components for SOI that belong to probability simplices with eigenbases rotated w.r.t. a fixed basis. Comparing density operators belonging to probability simplices with different eigenbases is a fundamental difference between classical and quantum fidelity measures. With this completed formalism, one could study quantum fidelity using a geometric approach provided by the SOI.

Given an orthonormal basis $\{ |(\lambda_S^\rho)^i\rangle \}$ of \mathcal{H}_S , all unitarily related orthonormal bases can be generated by

$$\{ |(\lambda_S^\sigma)^i\rangle \} = \{ U_S |(\lambda_S^\rho)^i\rangle \}. \quad (46)$$

This gives the set of all unitarily related probability simplices \mathcal{S}^ρ and \mathcal{S}^σ in $\mathcal{P}(\mathcal{H}_S)$ depicted in Fig. 10. From here, the set of purifications associated with a density operator

$$\sigma = \sum_{i=1}^N (\lambda^\sigma)^i |(\lambda_S^\sigma)^i\rangle \langle (\lambda_S^\sigma)^i|, \quad (47)$$

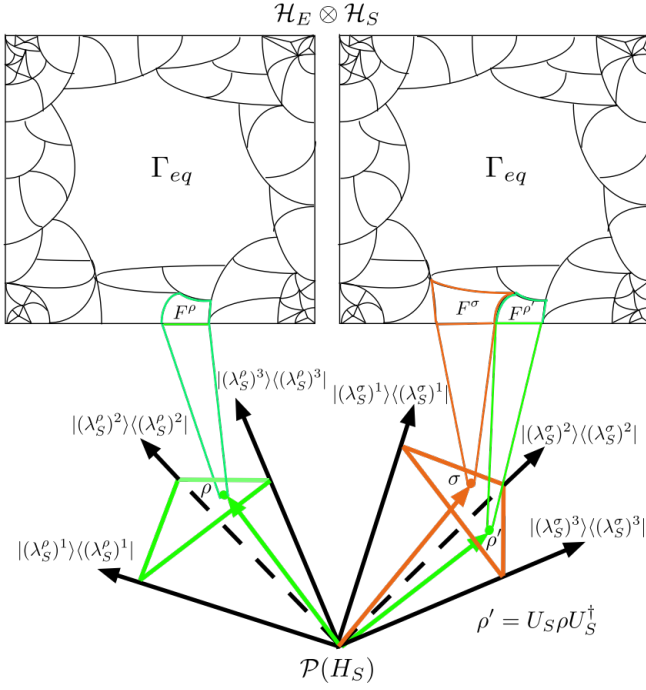


FIG. 10. Depiction of generalized entanglement coarse-graining procedure to allow unitary transformations of \mathcal{S} in $\mathcal{P}(\mathcal{H}_S)$. The green simplex on the left associated with ρ is \mathcal{S}^ρ and the orange simplex on the right associated with σ is \mathcal{S}^σ . The orthonormal basis of \mathcal{S}^σ is generated from unitary transformations U_S applied to the orthonormal basis of \mathcal{S}^ρ . Each simplex has a coarse-graining of \mathcal{H}_{ES} associated with them which are identical.

where $\vec{\lambda}^\sigma$ are free to be chosen independent of $\vec{\lambda}^\rho$, are given by (compare to Eq. 7)

$$|\vec{\Gamma}^\sigma(\vec{\xi})\rangle = (U_E(\vec{\xi}) \otimes \sqrt{\sigma})|\Gamma_{ES}^\sigma\rangle \quad (48)$$

where (compare to Eq. 6)

$$|\Gamma_{ES}^\sigma\rangle = \sum_{i=1}^N |(\lambda_E^\sigma)^i\rangle |(\lambda_S^\sigma)^i\rangle. \quad (49)$$

Like Eq. 6, $\{|(\lambda_E^\sigma)^i\rangle\}$ is a copy of $\{|(\lambda_S^\sigma)^i\rangle\}$ in \mathcal{H}_E . Now one simply inserts Eq. 48 into Eq. 11 to get the metric components of the surfaces of ignorance associated with \mathcal{S}^σ .

This generalization may give new insights into quantum fidelity. The standard fidelity measure between arbitrary quantum states is the Uhlmann-Josza fidelity [33]. It has many equivalent definitions two of which are given by

$$\mathcal{F}_{UJ} := \max_{\{U_S\}} |\text{Tr}[\sqrt{\rho}\sqrt{\sigma}U_S^T]|^2 \quad (50)$$

$$= \max_{\{\vec{\xi}_\rho, \vec{\xi}_\sigma\}} |(\vec{\Gamma}^\rho(\vec{\xi}_\rho)|\vec{\Gamma}^\sigma(\vec{\xi}_\sigma))|^2 \quad (51)$$

which are equations 9.110 and 9.97 in [1], respectively. If ρ and σ share the same eigenbasis, Eq. 50 reduces to the

classical fidelity between the eigenvalue spectrums of ρ and σ . This means that the difference between classical and quantum fidelity is the relationship between unitarily related eigenbases. Additionally, Eq. 51 shows that the Uhlmann-Josza fidelity can also be understood as an optimization over the surfaces of ignorance. Therefore, the generalized ECG may provide new geometric insights into quantum fidelity as it relates to the ECG.

V. CONCLUSION

In this paper, we introduced a new volume to quantify the amount of missing information or ignorance in a density operator ρ_S . This volume was computed by generating all purifications of ρ_S and constructing the metric tensor associated with the manifold of purifications. We denoted these manifolds as surfaces of ignorance (SOI). The determinant of the metric provides a volume element which is integrated to compute volume. Examples of the volume were provided for systems whose purifications were generated by Lie groups $SU(2)$, $SO(3)$, and $SO(N)$. In these examples, the volumes were studied in the context of an entanglement based quantum coarse-graining (CG) that we called the entanglement coarse-graining (ECG). This is a natural setting for studying the SOI since ρ_S can be understood as the reduced density operator of a pure state thus making its von Neumann entropy the entanglement entropy between system, S , and environment, E .

In the context of the ECG where the SOI are macrostates and purifications are microstates, we showed that our volumes captured two features of Boltzmann's original CG. These features are essential to typicality arguments used to understand thermalization and the 2nd law of thermodynamics. These features are (1) a system beginning in an atypical macrostate of smaller volume evolves to macrostates of greater volume until it reaches the equilibrium macrostate, and (2) the equilibrium macrostate takes up the vast majority of the coarse-grained space especially as dimension of the total system becomes large. Feature (1) was demonstrated by showing that the volume behaves like the von Neumann entropy in that it is zero on pure states, maximal on maximal mixed states, and is a concave function w.r.t the purity of ρ_S . This was shown in Figs. 3 and 4 for the $SU(2)$ and $SO(3)$ examples, respectively. Feature (2) was demonstrated by Fig. 6 for $SO(3)$ and extended using $SO(N)$ in Figs. 8 and 9.

The purpose of this work was not to study thermalization. Instead, we used information based “thermalization” as context to study our volumes in terms of the ECG. By demonstrating features (1) and (2) of the Boltzmann CG, we provided evidence that the intuitive understanding of the volume as a quantification of the missing in ρ_S is reasonable. Furthermore, it suggests that viewing these volumes as a multiplicity for an information/entanglement based “thermalization” entropy con-

stitutes a valid perspective. The ECG is also interesting in that it provides clear macro and microstates for the entanglement entropy. Because of this, the equilibrium macrostate is consistent with maximum entanglement between the S and E.

For future research, it would be interesting to study the well-known fact that most pure states of composite systems of high dimensions are close to maximally entangled [34] using the ECG. In the context of the ECG, this is simply an observation that the vast majority of the coarse-grained space of pure states consists of the equilibrium macrostate. This is feature (2) that was demonstrated in the examples of this paper and it is an essential feature of the results in [17–20, 35]. It would also be interesting to study the relationship between the ECG and the analysis in [36] since the microstates of the ECG are envariant (entanglement assisted invariant) states as described in [36]. Lastly, this research could be extended by defining a proper quantum Boltzmann entropy for the ECG. This is challenging since the volume goes to zero for pure states which means simply taking the logarithm of the volume would result in a divergent entropy.

ACKNOWLEDGMENTS

The authors wish to thank Christopher C. Tison and James E. Schneeloch for many useful discussions and inputs. PMA would like to acknowledge support of this work from the Air Force Office of Scientific Research (AFOSR). CC is grateful to the United States Air Force Research Laboratory (AFRL) Summer Faculty Fellowship Program for providing support for this work under grant #FA8750-20-3-1003. Any opinions, findings and conclusions or recommendations expressed in this material are those of the author(s) and do not necessarily reflect the views of Air Force Research Laboratory.

- [1] M. Wilde, *Quantum Information Theory*, Quantum Information Theory (Cambridge University Press, 2013).
- [2] J.M. Deutsch, “Thermodynamic entropy of a many-body energy eigenstate,” *New J. Phys.* **12**, 075021 (2010).
- [3] Lea F. Santos, Anatoli Polkovnikov, and Marcos Rigol, “Weak and strong typicality in quantum systems,” *Phys. Rev. E* **86**, 010102(R) (2012).
- [4] J.M. Deutsch, Haibin Li, and Auditya Sharma, “Microscopic origin of thermodynamic entropy in isolated systems,” *Phys. Rev. E* **87**, 042135 (2013).
- [5] Adam M. Kaufman, Eric M. Tai, Alexander Lukin, Matthew Rispoli, Robert Schittko, Philipp M. Preiss, and Markus Greiner, “Quantum thermalization through entanglement in an isolated many-body system,” *Science* **353**, 6301 (2016).
- [6] Dominik Safranek, J.M. Deutsch, and Anthony Aguirre, “Quantum coarse-graining entropy and thermalization in closed systems,” *Phys. Rev. A* **99**, 012103 (2019).
- [7] C. Duarte, G. D. Carvalho, N. K. Bernardes, and F. de Melo, “Emerging dynamics arising from coarse-grained quantum systems,” *Phys. Rev. A* **96**, 032113 (2017).
- [8] O. Kabernik, “Quantum coarse graining, symmetries, and reducibility of dynamics,” *Phys. Rev. A* **97**, 052130 (2018).
- [9] Pedro Silva Correia, Paola Concha Obando, O. Raul Vallejos, and Fernando de Melo, “Macro-to-micro quantum mapping and the emergence of nonlinearity,” *Phys. Rev. A* **103**, 052210 (2021).
- [10] Pedro Silva Correia and Fernando de Melo, “Spin-entanglement wave in a coarse-grained optical lattice,” *Phys. Rev. A* **100**, 022334 (2019).
- [11] Gabriel Dias Carvalho and Pedro Silva Correia, “Decay of quantumness in a measurement process: Action of a coarse-graining channel,” *Phys. Rev. A* **102**, 032217 (2020).
- [12] Carlos Pineda, David Davalos, Carlos Viviescas, and Antonio Rosado, “Fuzzy measurement and coarse graining in quantum many-body systems,” *Phys. Rev. A* **104**, 042218 (2021).
- [13] Jos Uffink, “Boltzmann’s Work in Statistical Physics,” in *The Stanford Encyclopedia of Philosophy*, edited by Edward N. Zalta (Metaphysics Research Lab, Stanford University, 2017) Spring 2017 ed.
- [14] Sheldon Goldstein, David A. Huse, Joel L. Lebowitz, and Roderich Tumulka, “Macroscopic and microscopic thermal equilibrium,” *Annalen der Physik* **529**, 1600301 (2017).
- [15] Sheldon Goldstein, *Chance in physics: Foundations and Perspectives* (Springer Berlin Heidelberg, 2001) pp. 39–54.
- [16] Sheldon Goldstein, Joel L. Lebowitz, Roderich Tumulka, and Nino Zanghi, *Statistical mechanics and scientific explanation: determinism, indeterminism and laws of nature* (World Scientific Publishing Co., 2020) p. 519.
- [17] Sheldon Goldstein, Joel L. Lebowitz, Roderich Tumulka, and Zanghi Nino, “Canonical typicality,” *Phys. Rev. Lett.* **96**, 050403 (2006).
- [18] Sheldon Goldstein and Roderich Tumulka, “On the approach to thermal equilibrium of macroscopic quantum systems,” *AIP Conference Proceedings* **1332**, 155 (2011).
- [19] H. Tasaki, “Typicality of thermal equilibrium and thermalization in isolated macroscopic quantum systems,” *J. Stat. Phys.* **163**, 937–997 (2016).
- [20] Sandu Popescu, Anthony J. Short, and Andreas Winter, “Entanglement and the foundations of statistical mechanics,” *Nature Phys* **2**, 754–758 (2006).
- [21] Ludwig Boltzmann, *Lectures on Gas Theory* (Berkeley: University of California Press, 1964).
- [22] Oscar E. Landford, *Statistical Mechanics and Mathematical Problems, Lecture Notes in Physics vol. 2.* (Springer-Verlag, 1973) pp. 1–113.
- [23] Koji Maruyama, Franco Nori, and Vlatko Vedral, “Colloquium: The physics of Maxwell’s demon and information,” *Rev. Mod. Phys.* **81**, 1 (2009).
- [24] L. Brillouin, “Maxwell’s demon cannot operate: Information and entropy: I,” *Journal App. Phys.* **22**, 334 (1951).
- [25] Erwin Schrödinger, *What is Life? The physical aspect of the living cell* (Cambridge University Press, 1944).
- [26] L. Brillouin, *Science and information theory*, 2nd ed. (Dover publications, 2013).
- [27] E. T. Jaynes, “Information theory and statistical mechanics,” *Phys. Rev.* **106**, 620–630 (1957).
- [28] K. Zyczkowski and M. Kus, “Random unitary matrices,” *J. Phys. A: Math. Gen.* **27**, 4235 (1994).
- [29] K. Zyczkowski, P. Horodecki, A. Sanpera, and M. Lewenstein, “Volume of the set of separable states,” *Phys. Rev. A* **58**, 2 (1998).
- [30] I. Bengtsson and K. Zyczkowski, *Geometry of quantum states: An introduction to quantum entanglement*, 2nd ed. (Cambridge University Press, 2017).
- [31] The method for associating volume (or entropy) with a discrete density operator ρ_l is only valid when ρ_l is close to a regular polygon. Since the mapping from the $\vec{\eta}$ basis to the $\vec{\lambda}$ basis creates elongated triangles, the value of volume (or entropy) at the center is no longer representative of ρ_l . This can be seen in the second row of Fig. 6 where the corner associated with the triangles is mono-colored while the corners consisting of more regular polygons have a clear gradient in color. The errors in counting which ρ_l belong to which L_a are ameliorated when triangular ρ_l are not considered. And since \mathcal{S} is symmetric, their removal does not affect the results.
- [32] A $D \times D$ matrix g_{ij} has $D!$ terms in the expansion of its determinant $\text{Det}(\mathbf{g})$. $SU(N)$ ($SO(N)$) has dimension $D = N^2 - 1$ ($(N(N - 1)/2)$). Thus $SU(3)$ with $D = 8$ has $8! = 40,320$ terms in $\text{Det}(\mathbf{g})$ which we were unsuccessful in analytically simplifying in *Mathematica*. $SO(3)$ with $D = 3$ has $3! = 6$ terms in $\text{Det}(\mathbf{g})$, while $SO(4)$ with $D = 6$ has $6! = 720$ terms, both of which can be simplified analytically.
- [33] Richard Jozsa, “Fidelity for mixed quantum states,” *Journal of modern optics* **41**, 2315–2323 (1994).
- [34] Patrick Hayden, Debbie W. Leung, and Andreas Winter, “Aspects of generic entanglement,” *Commun. Math. Phys.* **265**, 95–117 (2006).
- [35] Seth Lloyd, *Black holes, demons and the loss of coherence: how complex system get information, and what they do with it* (Rockefeller University, 1988) Chap. 3.
- [36] Sebastian Deffner and H. Wojciech Zurek, “Foundations of statistical mechanics from symmetries of entanglement,” *New J. Phys.* **18**, 063013 (2016).